

ARTICLE

Depolymerization of Organosolv Lignin over Silica-alumina Catalysts

Qing-yun Wu^{a,b}, Long-long Ma^{a,b}, Jin-xing Long^b, Ri-yang Shu^{b,c}, Qi Zhang^b, Tie-jun Wang^b, Ying Xu^{b*}

a. Department of Chemistry, University of Science and Technology of China, Hefei 230026, China

b. Key Laboratory of Renewable Energy, Guangzhou Institute of Energy Conversion, Chinese Academy of Sciences, Guangzhou 510640, China

c. University of Chinese Academy of Sciences, Beijing 100049, China

(Dated: Received on January 26, 2016; Accepted on May 26, 2016)

Efficient conversion of lignin to fine chemicals and biofuel become more and more attractive in biorefinery. In this work, we used a series of silica-alumina catalysts (*i.e.*, SiO₂-Al₂O₃, HY, H β , and HZSM-5) to degrade lignin into arenes and phenols. The relationship between the catalyst structure and lignin depolymerization performance was investigated. The results showed that both acidity and pore size of the catalyst could influence the conversion of lignin. In the volatilizable product, phenols were identified as the main phenolic monomers via gas chromatography-mass spectrometer. SiO₂-Al₂O₃ was the most efficient catalyst, giving 90.96% degree of conversion, 12.91% yield of phenols, and 2.41% yield of arenes in ethanol at 280 °C for 4 h. The Fourier transform infrared spectroscopy and ¹H nuclear magnetic resonance spectroscopy analysis demonstrated that deoxygenation and alkylation occurred in this process. The effect of solvents was also investigated and the results showed that ethanol was the most efficient solvent.

Key words: Lignin, SiO₂-Al₂O₃, Phenols, Deoxygenation, Alkylation

I. INTRODUCTION

Lignin, which consists of phenylpropane units of hydroxyphenyl (H), guaiacyl (G), and syringyl (S), is one of the main components of lignocellulose and the most abundant natural renewable aromatic resource. The depolymerization product from lignin can be used for bulk fine chemicals or precursor of biofuel. However, most lignin in pulping and biorefinery industry is burned as generation of heat currently [1–3]. Hence, efficient catalytic depolymerization of lignin into aromatic monomers is very important and necessary in conversion of biomass.

Conventional techniques of catalytic depolymerization of lignin include catalytic hydrogenolysis, base catalyzed depolymerization (BCD) process and catalytic fast pyrolysis *etc.* [4–6]. In catalytic hydrogenolysis, many supported metal catalysts are involved. Yan and his co-workers degraded wood lignin selectively to C₉ or C₁₈ alkanes over noble metal [7]. The lignin could be degrade to monomers and dimer, and then monomers or dimers was converted to C₉ or C₁₈ alkanes. The selectivity of C₉ and C₁₈ alkanes could be 85.4% and 59.9% over Pd/C and H₃PO₄ under optimized condition respectively. Li and his workers used Mo-based cata-

lysts to degrade lignin to high-value chemicals efficiently [8–10]. For instance, using α -molybdenum carbide catalyst in pure ethanol at 280 °C, high-value chemicals of low molecular weight was obtained with a maximum overall yield of 25 most abundant liquid products (which consisted of C₆-C₁₀ esters, alcohols, arenes, phenols, and benzyl alcohols) of 1.64 g per gram of lignin. In our previous work [11], lignin could be depolymerized in the presence of Pd/C cooperated with metal chlorides catalysts and more than 35.4% yield of phenolic monomers could be obtained. Generally, high yield of product could be obtained using these noble metal catalysts, but in these processes, the involvement of noble metal makes it expensive.

The BCD process is much more economical. NaOH, KOH, and K₂CO₃ were ordinary base catalysts for the lignin depolymerization [12]. Using different bases, various product yields and components could be obtained. However, most base catalysts for lignin depolymerization are homogeneous, such as NaOH and KOH, which is not recyclable on catalytic reaction.

Considering most linkages in the structure of lignin are the β -O4 and α -O4 linkages [13], acidolysis can be an efficient process for depolymerization of lignin due to its strong ability to break C–O bond. In early work [14, 15], both homogeneous and heterogeneous acid catalysts were used in mechanistic instigation of cleavage of β -O4 model compounds and depolymerization of lignin into aromatic monomers. In this work, amorphous silica-alumina and zeolites such as HY, H β ,

* Author to whom correspondence should be addressed. E-mail: xuying@ms.giec.ac.cn, Tel.: +86-20-87048614, FAX: +86-20-87057751

and HZSM-5, which were widely used in the cracking of fossil oil and biomass, were utilized as solid catalysts in depolymerization of lignin. The effect of structure of the catalysts were examined. The structure evolution was also investigated via the comparison analysis of the raw lignin and products. Methanol, tetrahydrofuran (THF), isopropanol (*i*-PrOH), and ethanol were also investigated in order to understand the effects of solvents.

II. EXPERIMENTS

A. Materials

SiO₂-Al₂O₃ was purchased from Sigma Aldrich. HY, H β , and HZSM-5 were supplied by the catalyst plant of Nankai University. Methanol, ethanol, *i*-PrOH, and THF were analytical grade and purchased from Guanghua chemical factory Co., Ltd. (Shantou). The pennisetum lignin was separated according to previous literature [16], and it was soluble very well in ethanol. The dilute acid hydrolysis experiment showed that not any sugar was not detected. Elemental analysis demonstrated that it contained 63.8% C, 5.76% H, 29.09% O, 0.51% N, and 0.81% S.

B. Characterization of catalysts

All catalysts were calcined for 4 h at 550 °C. The properties of catalysts were characterized by NH₃ temperature programmed desorption (NH₃-TPD). The profiles of NH₃-TPD was obtained on a ChemBET pulsar TPR/TPD automated chemisorption analyzer. Each catalyst was first treated at 550 °C for 90 min in He flow of 70 mL/min, and then cooled to room temperature, exposed to 20%NH₃/He for 60 min, and purged in He for 60 min at 100 °C. Temperature ramped to 750 °C at 5 °C/min. The brunauer-emmett-teller surface area and pore size of catalysts were obtained on a micro-metric ASAP-2010 automated system by N₂ isothermal (77 K) absorption.

C. Lignin depolymerization

In a typical depolymerization reaction, 0.5 g lignin, 40 mL ethanol, and 0.5 g catalyst were added into a 100 mL batch autoclave equipped with a mechanical agitation in sequence. After the air replacement of N₂ for three times, the reactor was sealed and heated to the desired temperature for a certain time. When the reaction was finished, the reactor was cooled to room temperature.

D. Products separation and analysis

After depolymerization, the product was first filtered, then the solid residues were washed by ethanol for three

times. At last, mixing the eluent and filtrate, water was added in the mixture to recover the lignin.

The volatile products were identified using an Agilent 5890 gas chromatography (GC) with an Agilent 5975 inelt mass-selective detector according to the NIST MS library. The quantitative analysis of the volatile product was detected by SHIMADZU GC2014C with a flame ionization detector (FID) and acetophenone was used as internal standard chemical. The gas chromatography-mass spectrometer (GC-MS) and GC were equipped with the same column (HP-INNOWAX (30 m×0.25 mm×0.25 μ m)), and shared the same oven temperature program (60 °C hold for 2 min, and then ramp to 260 °C with 10 °C/min, and hold for extra 10 min. The temperature of injector was 280 °C in split mode with split ratio of 5:1). The measurement of molecular weight distribution of product was conducted on Waters 2695 high performance liquid chromatography apparatus. THF was used as eluent with the flow rate of 1.0 mL/min. The injected volume was 50 μ L, and the column was kept at 30 °C. Polystyrene was used as standard chemical. The Fourier transform infrared spectroscopy (FT-IR) spectrum was obtained on a Nicolet 50 FT-IR spectrometer using KBr pelleting method. ¹H nuclear magnetic resonance spectroscopy (¹H-NMR) was conducted on a Bruker AVANCE III 300 WB spectrometer (7.05 T). The thermogravimetric analysis (TGA) were obtained on TGA Q50 (ramped up from 30 °C to 850 °C at 10 °C/min in nitrogen) and scanning electron microscope (SEM) images were obtained on a Hitach S-4800 instrument.

E. Measurement of products

The degree of conversion was obtained by weight comparison of recovered lignin and the original lignin as shown in Eq.(1). The volatile products was determined and measured by GC-MS and GC, respectively. Acetophenone was used as internal standard chemical. The yield of arenes and phenols was calculated as follows:

$$\text{Degree of conversion} = \frac{W_F - W_R}{W_F} \times 100\% \quad (1)$$

$$\text{Yield of solid residue} = \frac{W_S}{W_F} \times 100\% \quad (2)$$

$$\text{Yield of arenes} = \frac{W_A}{W_F} \times 100\% \quad (3)$$

$$\text{Yield of phenols} = \frac{W_P}{W_F} \times 100\% \quad (4)$$

where W_F is the weight of feed lignin, W_R is the weight of recovered lignin, W_S is the weight of solid residue, W_A is the weight of arenes, W_P is the weight of phenols.

TABLE I Characterization of BET of catalysts.

Catalysts	$S_{\text{BET}} / (\text{m}^2/\text{g})$	$V_p / (\text{cc}/\text{g})$	d_p / nm
HY	574.1	0.1	3.4
$\text{SiO}_2\text{-Al}_2\text{O}_3$	459.4	0.6	4.3
H β	492.2	0.1	3.1
HZSM-5	383.8	0.1	3.7

Note: S_{BET} is BET surface, V_p is pore volume, d_p is pore diameter.

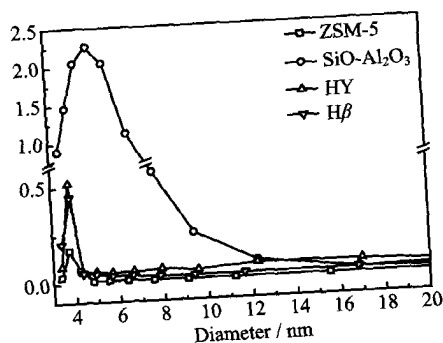


FIG. 1 The pore size distribution of catalysts.

III. RESULTS AND DISCUSSION

A. Characterization of catalysts

The characterizations of catalysts were shown in Table I, Fig.1, and Fig.2.

According to the analysis of BET surface and pore size distribution, it was known that the BET surface areas ranged from 383.8 m^2/g to 574.1 m^2/g . Among the catalysts, HY had the largest BET surface areas, and $\text{SiO}_2\text{-Al}_2\text{O}_3$ had largest pore size. With the pore volume and diameter being 0.6 cc/g and 4.3 nm, much larger than those of other catalysts.

According to the position of desorption peak in the profiles of $\text{NH}_3\text{-TPD}$ of the catalysts, the acidity strength of catalysts could be determined and higher desorption temperature of NH_3 indicated stronger acidity [17]. As shown in Fig.1, the $\text{NH}_3\text{-TPD}$ profiles of $\text{SiO}_2\text{-Al}_2\text{O}_3$, and HZSM-5 showed two obvious peaks assigned to medium acid sites and strong acid sites. The $\text{NH}_3\text{-TPD}$ profiles of HY and H β had only one peak in range of 150–450 $^\circ\text{C}$. Comparing the first desorption peak of $\text{NH}_3\text{-TPD}$ profiles of different catalysts, HZSM-5 and H β had relatively stronger acidity, and HY had the weakest acidity.

The XRD patterns of catalysts were also conducted and shown in Fig.3. Except $\text{SiO}_2\text{-Al}_2\text{O}_3$, intense peaks were obviously observed. $\text{SiO}_2\text{-Al}_2\text{O}_3$ was amorphous, and others were crystalline.

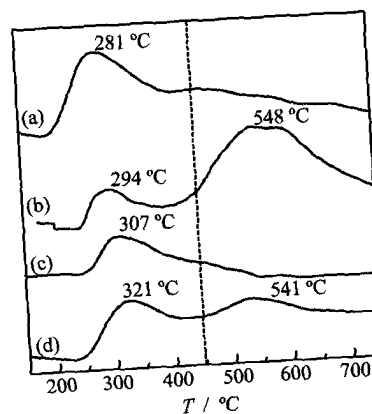
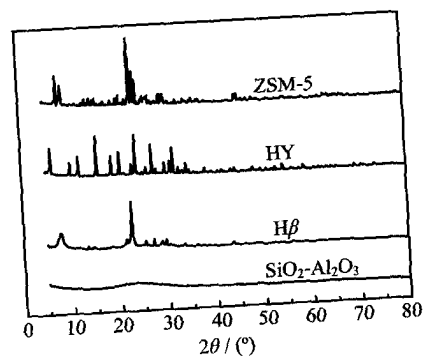
FIG. 2 The $\text{NH}_3\text{-TPD}$ profiles of catalysts.

FIG. 3 XRD patterns of various catalysts.

B. Analysis of gas products

After the depolymerization reaction of lignin, the gas product was collected and identified by GC-TCD-FID using external standard method. Results showed that the gas products contained H_2 , CH_4 , CO , and CO_2 , which might come from the decomposition of methoxy, carbonyl and carboxyl groups in lignin structure. Yields of CH_4 , CO_2 , and CO are shown in Table II. It was known that the highest yields of CO_2 and CO were obtained over H β , and when $\text{SiO}_2\text{-Al}_2\text{O}_3$ used, less CO_2 and CO were obtained. Some hydrocarbons ($\text{C}_2\text{-C}_6$) were also detected, which could be generated by conversion of ethanol catalyzed by these catalysts [18].

C. Analysis of liquid products

1. Analysis of volatile liquid product

The liquid products from lignin depolymerization were identified by GC-MS. It showed that more than 10 kinds of chemical were detected, in which most products were aromatic hydrocarbons and phenolic monomers. Aromatic hydrocarbon observed such as ethylbenzene and 1,3-diethyl-5-methyl-benzene could be defined as deoxygenated and alkylated products derived

TABLE II Yield of CH₄, CO₂, and CO.

Catalysts	Yield/%		
	CH ₄	CO ₂	CO
HY	1.76	2.02	1.28
SiO ₂ -Al ₂ O ₃	0.32	0.52	0.22
H β	4.35	5.10	3.19
HZSM-5	1.63	2.46	1.18

lignin, suggesting that serious alkylation occurred in this work (Table S1). Phenolic monomers from the depolymerization of lignin included phenols, guaiacols, and syringols. Syringols could be transformed into guaiacols and then to phenols [19]. Phenols were much steadier than the other two. In this catalytic process, the transformation could happen and phenols were the major components of phenolic monomers. Meanwhile, some naphthenic compounds were detected according to the result of GC-MS, which could be also identified in catalytic pyrolysis of lignin [20]. The reform reaction could happen. It suggested that in this catalytic process, silica-alumina could not only catalyze lignin degraded to phenolic monomer, but also promote deoxygenation, alkylation, and reform reaction. Some aromatic compounds with carbonyl groups such as 1-(2-hydroxy-5-methylphenyl)-ethanone, could be products by cleavage of β -O4 in lignin [21].

Table III shows the depolymerization of organosolv lignin over these typical silica-alumina catalysts we used. Without catalyst, the conversion degree of lignin could be 60.16% but the yield of solid residue reached the highest point with 45.84%, which indicated that without catalysts, thermal effect caused serious repolymerization. However, with catalysts being added, the repolymerization was suppressed. Lower yield of solid residue was obtained, but the conversion of lignin and the yields of arenes and phenols had a significant increase (Table III, entries 2-5). Considering the properties of the catalysts, acidity and pore size could impact depolymerization. HY had relatively weaker acidity, and 8.32% yield of phenols was obtained. Among the catalysts we chose, HZSM-5 and H β had higher acidity, but both of them showed lower activity in conversion of lignin to arenes and phenols, where only 4.60% and 4.69% yield of phenols were given respectively. It seemed that either weaker or stronger acidity could not favor converting lignin to arenes and phenols. On the contrary, SiO₂-Al₂O₃ with moderate acidity was more efficient than other catalysts and the highest yield of phenols (12.91%, Table III, entry 3) was obtained. Generally, with the acidity of catalysts increasing, the yield of solid residue decreased, indicating that stronger acidity could suppress the repolymerization into solid residue, and moderate acidity could promote the depolymerization of lignin into phenolic monomers. Also, with lignin being degraded, some unstable intermedi-

ates were formed, which could repolymerize to oligomer or be stabilized to phenols and arenes. It was supposed that the stabilization of intermediates occurred in the pore of catalysts in the presence of the catalysts [22]. Larger pore size of catalysts make reactive intermediates enter and stabilized more easily. So SiO₂-Al₂O₃ with the largest pore and moderate size was the most efficient catalyst.

2. Analysis of nonvolatile liquid product

The molecular weight distribution of the raw lignin and the nonvolatile products over various catalysts were also investigated using GPC analysis in Table IV.

As shown in Table IV, after depolymerization, all products had M_n in range of 590–930, lower than that of raw lignin. Here, under catalysis of HZSM-5 and H β , the products had higher average molecular. Especially, when HY and SiO₂-Al₂O₃ used, the products having lowest M_n were obtained. According to element analysis, a monomer molecular of organosolv lignin could be C₉H_{9.75}O_{2.73}N_{0.07}S_{0.04}, and its molecular weight could be 163. It indicated that under catalysis of HY and SiO₂-Al₂O₃, besides phenolic monomers, most of the products were trimers and tetramers. As discussed above, HZSM-5 and H β showed low activity in conversion of lignin because of their higher acidity.

To understand the structure change between raw lignin and the nonvolatile product, FT-IR and ¹HNMR characterization were conducted (Fig.4 and Table V).

The FT-IR spectrum of raw lignin showed that a wide and intense peak at 3401 cm⁻¹, which was assigned to the stretching vibration of hydroxyl group in lignin. The peak at 2926 cm⁻¹ was assigned to the structure of aliphatic C–H in lignin [16]. The shape and intense peak at 1710 cm⁻¹ was the characteristic absorption of the carbonyl group in lignin structure. Three peaks at 1605, 1514, and 1457 cm⁻¹ were assigned to aromatic skeleton vibration which was the fundamental structure of lignin. Peaks at 846 and 1116 cm⁻¹ indicated the guaiacyl structure in lignin molecule [19]. The FT-IR spectra of products from lignin depolymerization over silica-alumina catalysts showed obvious difference from the raw lignin. Except HZSM-5, the significant increase of the peak strength at 2965 and 2846 cm⁻¹, which were assigned to the structure of -CH₃ and -CH₂- respectively, suggesting the alkyl group generation after catalytic reaction. It accorded well with the above GC-MS results that alkylated compounds such as propofol were detected in the liquid product. The peak at 1710 cm⁻¹ which could be clearly observed in the spectrum of raw lignin decreased obviously. When H β was used, the peak assigned to carbonyl could not be detected in the spectrum of product and the highest yields of CO and CO₂ were obtained. It indicated that the serious decarboxylation happened and most carbonyl group in raw lignin was converted to CO₂ or CO.

According to previous work, the ¹HNMR spectra of

TABLE III Catalytic depolymerization of organosolv lignin over various catalysts.

Entry	Catalyst	Conversion of lignin/%	Yield/%		
			Arenes	Phenols	Solid residue
1	None	60.16	0.76	2.03	45.84
2	HY	85.74	1.89	8.32	25.44
3	SiO ₂ -Al ₂ O ₃	90.96	2.41	12.91	18.04
4	H β	87.05	3.01	4.69	14.95
5	HZSM-5	95.46	2.40	4.60	12.54

TABLE IV Average molecular weight of products.

Catalysts	M_n	M_w	D
Raw lignin	1033	1630	1.57
HY	599	682	1.13
SiO ₂ -Al ₂ O ₃	560	665	1.18
H β	851	1435	1.69
HZSM-5	897	1439	1.61

Note: M_n is number average molecular weight, M_w is weight average weight, and D is dispersion degree.

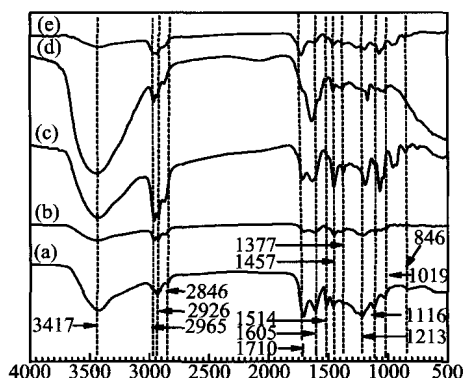


FIG. 4 FT-IR spectra of (a) raw lignin and the nonvolatile products over different catalysts: (b) HY, (c) SiO₂-Al₂O₃, (d) H β , and (e) HZSM-5.

both raw lignin and product could be divided to some sections of 0.3–2.3, 2.6–5.0, and 6.0–8.5 ppm [19, 23]. Peaks at the range of 0.3–2.3 ppm were assigned to aliphatic protons. The chemical shift ranged at 2.6–5.0 and 6.0–8.5 ppm were assigned to oxygenated side chain and aromatic proton, respectively. According to integration distributions of protons, we could know the transformation of protons in this process. As for raw lignin, the integration distributions of aliphatic protons, aromatic protons and protons on carbon that bear an oxygen were 33%, 54%, and 13%, respectively. After catalytic process, the integration of aliphatic protons increased which suggested that deoxygenation and alkylation occurred. Many oxygenated chains were destructed, which resulted in the deoxygenated product as detected by GC-MS. Methoxyl group was primary

function group in lignin, observed in structure of guaiacyl and syringyl groups, so it could be obviously detected, but this peak was weakened or disappeared in the ¹HNMR spectra of products in Fig.S1–S5 (supplementary materials). Furthermore, main product was phenol, and guaiacol and syringol could hardly be detected according to the GC-MS results. It indicated that methoxyl groups were removed from aromatic ring in this catalytic process.

D. Analysis of solid residue

In this reaction, depolymerization and repolymerization were a pair of competitive processes. When the repolymerization reaction occurred, the soluble initial lignin was converted to be insoluble in the solvent ethanol, and combined with the catalysts. The SEM images of raw lignin and the residues showed that the lignin residue was hardened lamellars after depolymerization, whereas raw lignin was loose spheres (Fig.5). The SEM images also showed that the solid residue over SiO₂-Al₂O₃ was porous, and the solid residues over other catalysts were denser than it. The depolymerization of lignin occurred at the surface of catalyst. When the solid residue covering catalyst was porous, the lignin dissolved in ethanol could still cross it and arrived at the active sites of catalyst. However when it was dense, the lignin could hardly arrive at the active sites and the depolymerization was suppressed. Hence, SiO₂-Al₂O₃ was the most active in this catalytic process. Furthermore, in catalytic process tar/char deposited at the catalytic sites of catalysts, causing catalysts deactivation. It was also considered to be a main reason for that SiO₂-Al₂O₃ was more efficient than other catalysts at last.

The thermochemical properties of raw lignin and solid residue were further investigated. A weight loss stage 100–850 °C could be observed in the TGA curve of raw lignin (Fig.6(a)). At 100 °C the weight loss could be attributed to the trace moisture and as temperature increasing, the lignin decomposed. When temperature was higher than 350 °C, the rate of weight loss was substantially increased. At the end of TGA curve, 59.02% of weight loss was shown. The TGA curves of solid residue after depolymerization over various catalysts were significantly different from the raw lignin. Compared with raw lignin, less weight loss was shown

TABLE V Relative quantification of protons by ^1H NMR.

Group	δ/ppm	Integration/%				
		lignin	HY	$\text{SiO}_2\text{-Al}_2\text{O}_3$	H β	HZSM-5
Aliphatic protons	0.3–2.3	33	60	42	47	41
Aromatic protons	2.6–5	54	34	48	50	57
Protons ^a	6.0–8.5	13	6	10	3	2

^a. Protons on carbon bearing an oxygen and -OH.

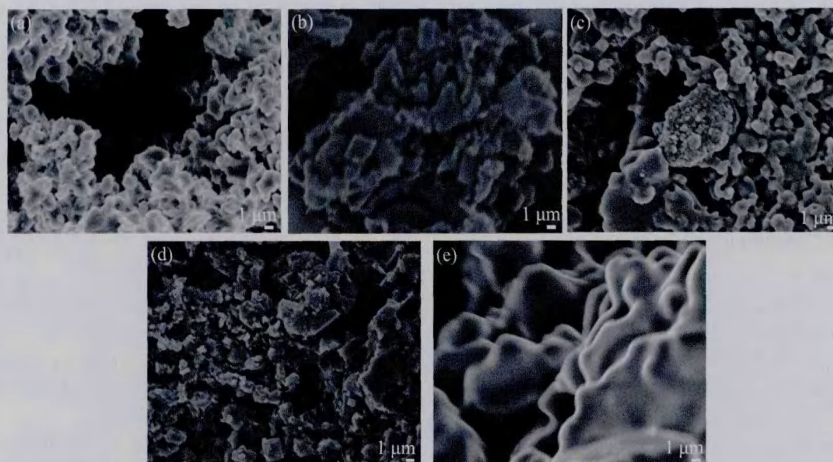


FIG. 5 The SEM images of (a) raw lignin, and products over different catalysts: (b) HY, (c) $\text{SiO}_2\text{-Al}_2\text{O}_3$, (d) H β , and (e) HZSM-5.

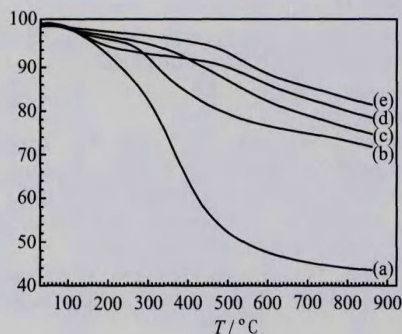


FIG. 6 TGA of (a) raw lignin, and solid residue after depolymerization with different catalysts: (b) HY, (c) $\text{SiO}_2\text{-Al}_2\text{O}_3$, (d) H β , and (e) HZSM-5.

due to the depolymerization of the loosen fraction of the lignin and were much more resistant to thermal decomposition. Furthermore, the TGA curves of the residues from various catalytic processes were also different from each other.

E. Effect of solvents over $\text{SiO}_2\text{-Al}_2\text{O}_3$

The effect of methanol, THF, *i*-PrOH, and ethanol were investigated for the depolymerization of lignin. Figure 7 shows the distribution of product. THF could

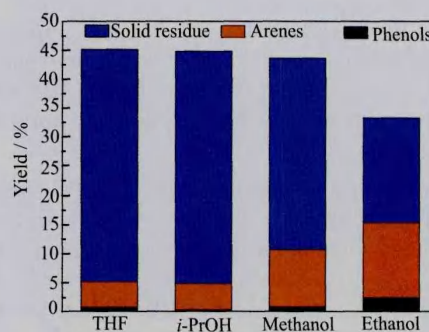


FIG. 7 The depolymerization of lignin over $\text{SiO}_2\text{-Al}_2\text{O}_3$ in different solvents.

be used as an efficient solvent or co-solvent for efficient conversion of lignin and lignocelluloses [24, 25]. However as cyclic ethers, THF could not generate active hydrogen under reaction conditions. In the presence of $\text{SiO}_2\text{-Al}_2\text{O}_3$, THF could also polymerize to polytetrahydrofuran [26], which might suppress depolymerization of lignin. Hence, when THF was used as solvent, only 0.7% and 4.45% yields of arenes and phenols were achieved, respectively. THF could not promote efficient conversion of lignin, but resulting in serious repolymerization in this catalytic process. As short aliphatic alcohols, methanol, ethanol, and *i*-PrOH could

generate active hydrogen or produce hydrogen under reaction conditions [27, 28]. These aliphatic alcohols were not only solvents but also involved in depolymerization. The solvolysis happened. Alcohol molecules could promote to cleavage of either bond in lignin structure and reacted with products from lignin. An appropriate alcohol makes depolymerization more efficient. Although *i*-PrOH could generate hydrogen, comparing with methanol and ethanol, *i*-PrOH has larger steric size. Hence, the yields of arenes and phenols in *i*-PrOH were much lower than those in methanol and ethanol. Meanwhile, it was reported that ethanol could be involved in alkylation reaction suppressing repolymerization [29]. In conclusion, higher yields of arene and phenols were obtained in methanol and ethanol.

IV. CONCLUSION

Orgnosolv lignin was efficiently converted to phenolic monomer over various silica-alumina catalysts. Among the catalysts, SiO₂-Al₂O₃ with moderate acid strength was found to be the most efficient. Phenols were the major components of phenolic monomers. When SiO₂-Al₂O₃ was used, 2.41% yield of arenes and 12.91% yield of phenols were obtained in an ethanol at 280 °C for 4 h. Catalyst characterization results showed that both acidity and pore size were the significant properties for lignin efficient conversion. Further investigation of the structure and physical-chemical properties of the original lignin and depolymerization products demonstrated that deoxygenation and alkylation occurred in the lignin depolymerization. The solvents impacted the depolymerization significantly. Ethanol and methanol were the most two efficient solvents for its relatively small steric size and excellent ability to supply active hydrogen.

Supplementary materials: Scheme S1 shows the proposal path of acid catalyzed depolymerization of lignin. Table S1 shows aromatic monomers of products over SiO₂-Al₂O₃ detected by GCMS analysis. Figure S1, S2, S3, S4, and S5 show ¹HNMR spectra of raw lignin, products over HY, products over HY, products over SiO₂-Al₂O₃, products over Hβ, and spectrum of products over HZSM-5, respectively.

V. ACKNOWLEDGMENTS

This work was supported by the National Key Technology R&D Program (No.2014BAD02B01) and the National Natural Science Foundation of China (No.51476178).

[1] J. Zakzeski, P. C. A. Bruijninx, A. L. Jongerius, and B. M. Weckhuysen, *Chem. Rev.* **110**, 3552 (2010).

- [2] A. J. Ragauskas, G. T. Beckham, M. J. Bidy, R. Chandra, F. Chen, M. F. Davis, B. H. Davison, R. A. Dixon, P. Gilna, M. Keller, P. Langan, A. K. Naskar, J. N. Saddler, T. J. Tschaplinski, G. A. Tuskan, and C. E. Wyman, *Science* **344**, 1246843 (2014).
- [3] P. Azadi, O. R. Inderwildi, R. Farnood, and D. A. King, *Renew. Sust. Energ. Rev.* **21**, 506 (2013).
- [4] Q. Song, F. Wang, and J. Xu, *Chem. Comm.* **48**, 7019 (2012).
- [5] X. Erdocia, R. Prado, M. Á. Corcuera, and J. Labidi, *Biomass Bioenergy* **66**, 379 (2014).
- [6] C. A. Chen, H. Pakdel, and C. Roy, *Bioresour. Technol.* **79**, 27 (2001).
- [7] N. Yan, C. Zhao, P. J. Dyson, C. Wang, L. T. Liu, and Y. Kou, *ChemSusChem* **1**, 626 (2008).
- [8] R. Ma, W. Hao, X. Ma, Y. Tian, and Y. Li, *Angew. Chem.* **53**, 7310 (2014).
- [9] X. Ma, K. Cui, W. Hao, R. Ma, Y. Tian, and Y. Li, *Bioresour. Technol.* **192**, 17 (2015).
- [10] X. Ma, R. Ma, W. Hao, M. Chen, F. Yan, K. Cui, Y. Tian, and Y. Li, *ACS Catal.* **5**, 4803 (2015).
- [11] R. Shu, J. Long, Z. Yuan, Q. Zhang, T. Wang, C. Wang, and L. Ma, *Bioresour. Technol.* **179** 84 (2015).
- [12] A. Toledano, L. Serrano, A. M. Balu, R. Luque, A. Pineda, and J. Labidi, *ChemSusChem* **6**, 529 (2013).
- [13] I. Klein, B. Saha, and M. M. Abu-Omar, *Catal. Sci. Technol.* **5**, 3242 (2015).
- [14] M. R. Sturgeon, S. Kim, K. Lawrence, R. S. Paton, S. C. Chmely, M. Nimlos, T. D. Foust, and G. T. Beckham, *ACS. Sustain. Chem. Eng.* **2**, 472 (2014).
- [15] A. K. Deepa and P. L. Dhepe, *ACS. Catal.* **5**, 365 (2015).
- [16] J. Long, W. Lou, L. Wang, B. Yin, and X. Li, *Chem. Eng. Sci.* **122**, 24 (2015).
- [17] S. Kirumakki, B. Shpeizer, G. Sagar, K. Chary, and A. Clearfield, *J. Catal.* **242**, 319 (2006).
- [18] A. Galadima and O. Muraza, *J. Ind. Eng. Chem.* **31**, 1 (2015).
- [19] B. Joffres, C. Lorentz, M. Vidalie, D. Laurenti, A. A. Quoineaud, N. Charon, A. Daudin, A. Quignard, and C. Geantet, *Appl. Catal. B* **145**, 167 (2014).
- [20] M. A. Jackson, D. L. Compton, and A. A. Boateng, *J. Anal. Appl. Pyrolysis* **85**, 226 (2009).
- [21] P. J. Deuss, M. Scott, F. Tran, N. J. Westwood, J. G. de Vries, and K. Barta, *J. Am. Chem. Soc.* **23**, 7456 (2015).
- [22] Z. Ma, E. Troussard, and J. A. van Bokhoven, *Appl. Catal. A* **423**, 130 (2012).
- [23] K. Barta, T. D. Matson, M. L. Fettig, S. L. Scott, A. V. Iretskii, and P. C. Ford, *Green. Chem.* **12**, 1640 (2010).
- [24] Z. Jiang, T. He, J. Li, and C. Hu, *Green. Chem.* **16**, 4257 (2014).
- [25] Y. Yang, C. W. Hu, and M. M. Abu-Omar, *Green. Chem.* **14**, 509 (2012).
- [26] Y. Y. Ge, Z. Q. Jia, C. G. Gao, L. L. Zhao, H. T. Li, Y. Zhang, and Y. X. Zhao, *Kinet. Catal.* **54**, 761 (2013).
- [27] Q. Song, F. Wang, J. Cai, Y. Wang, J. Zhang, W. Yu, J. Xu, *Energ. Environ. Sci.* **6**, 994 (2013).
- [28] J. R. S. G. A. Deluga, L. D. Schmidt, and X. E. Verykios, *Science* **303**, 993 (2004).
- [29] X. Huang, T. I. Koranyi, M. D. Boot, and E. J. Hensen, *ChemSusChem* **7**, 2276 (2014).

法

过渡金属掺杂在 $\text{Na}_{0.5}\text{Bi}_{0.5}\text{TiO}_3$ 体系中诱导产生磁性的第一性原理研究 462

鞠林^a, 徐同帅^a, 张雍家^b, 孙礼^{b*} (a. 安阳师范学院物理与电气工程学院, 安阳 455000; b. 太原理工大学物理系, 太原 030024)

摘要: 用从头算研究了在 $\text{Na}_{0.5}\text{Bi}_{0.5}\text{TiO}_3$ 体系中, 采用过渡金属掺杂从而诱导出磁性的可能性. 计算结果表明, 用一个过渡金属原子置换一个钛原子之后, 可以在该体系中产生磁矩. 所产生的磁矩主要是由于过渡金属原子的3d轨道电子的自旋极化导致的. 通过交换关联能的计算, 我们发现铬、锰、铁、钴掺杂的 $\text{Na}_{0.5}\text{Bi}_{0.5}\text{TiO}_3$ 体系中, 反铁磁耦合状态比铁磁耦合状态稳定. 印证了实验中, 随着锰、铁掺杂量的增加, $\text{Na}_{0.5}\text{Bi}_{0.5}\text{TiO}_3$ 体系在低温下铁磁性消失, 顺磁性增强. 在钒掺杂的 $\text{Na}_{0.5}\text{Bi}_{0.5}\text{Ti}_{0.67}\text{O}_3$ 体系中, 铁磁耦合比反铁磁耦合稳定, 并且带有 $2\mu_B$ 的磁矩. 这就意味着, 可以通过钒掺杂制备 $\text{Na}_{0.5}\text{Bi}_{0.5}\text{Ti}_{0.67}\text{O}_3$ 低温铁磁材料.

关键词: 过渡金属, 掺杂, 磁性, 第一性原理计算

活化气氛对钨基合成醇催化剂的结构和性能的影响 467

周纪龙^a, 谢威^a, 孙松^{a*}, 姬丽丽^a, 郑黎荣^b, 高琛^{a,c}, 鲍骏^{a,c*} (a. 中国科学技术大学, 国家同步辐射实验室, 化学能源材料协同创新中心, 合肥 230029; b. 中国科学院高能物理研究所, 北京 100039; c. 中国科学技术大学材料科学与工程学院, 中国科学院能源转换材料重点实验室, 合肥 230026)

摘要: 制备了活性炭负载的钨基催化剂, 采用三种不同的活化气氛对催化剂进行还原. 还原气包括纯氢, 合成气($\text{H}_2/\text{CO}=2/1$), 纯CO. 催化剂结构利用X射线衍射(XRD)、X射线吸收的精细结构光谱(XAFS)和原位的漫反射傅里叶变换红外光谱(in-situ DRIFTS)表征. 活化后催化剂低醇合成性能经过测试. 纯氢具有最强的还原能力, 导致催化表面生成更多的低价态的 $\text{Mo}^{\phi+}$ ($0 < \phi < 2$)物种和Co金属. CO的解离和氢化活性过高, 促进了烃的生成而降低了醇的选择性. 相比之下, CO还原的催化剂的还原程度相对弱, Mo、Co物种主要以 Mo^{4+} 和 Co^{2+} 形式存在. 合成气还原的催化剂表现最佳的低醇合成活性和选择性. 这说明合成气具有介于 H_2 和CO之间的合适还原能力, 导致催化表面丰富的 $\text{Mo}^{\delta+}$ 物种和多种价态的Co物种共存. 这些物种之间的协同作用, 平衡了CO解离、加氢和CO插入反应活性, 因而促进了低醇的生成.

关键词: 低醇合成, 活化机理, 原位漫反射傅里叶变换红外光谱, 钨基催化剂, 合成气

硅钨催化剂催化有机溶剂木质素的解聚 474

吴青云^a, 马隆龙^{a,b}, 龙金星^b, 舒日洋^{b,c}, 张琦^b, 王铁军^b, 徐莹^{b*} (a. 中国科学技术大学化学与材料科学学院, 合肥 230026; b. 中国科学院广州能源研究所, 广州 510640; c. 中国科学院大学, 北京 100049)

摘要: 使用一系列的硅钨催化剂($\text{SiO}_2\text{-Al}_2\text{O}_3$, HY, H β 和HZSM-5)催化解聚木质素转化为芳香烃和苯酚类化合物. 研究了催化剂结构和其解聚木质素性能之间的关系. 结果表明催化剂的酸性和孔道尺寸都会影响木质素解聚. 经气相色谱质谱联用检测, 发现产物中含量最主要的酚类产物是苯酚类化合物. $\text{SiO}_2\text{-Al}_2\text{O}_3$ 是效果最好的催化剂, 以它为催化剂时木质素转化率为90.96%, 芳香烃和苯酚类产物的收率分别为2.41%和12.91%. 产物的红外吸收光谱和核磁共振谱的分析也表明反应过程中发生了脱氧和烷基化反应. 最后也对溶剂对反应的影响进行了研究, 发现乙醇是最佳的反应溶剂.

关键词: 木质素, $\text{SiO}_2\text{-Al}_2\text{O}_3$, 苯酚类化合物, 脱氧反应, 烷基化反应

含氧有机物催化重整制备纯氢 481

薛鹤, 刘俊旭, 夏彤岩, 李全新* (中国科学技术大学化学物理系, 中国科学院城市污染物转化重点实验室, 安徽省生物质洁净能源重点实验室, 合肥 230026)

摘要: 研究了一种新的利用含氧化合物制备纯氢的催化变换过程, 该过程耦合了含氧化合物的催化重整、水煤气变换反应和 CO_2 去除步骤. 详细研究了重整催化剂的筛选、反应条件以及不同的含氧化合物催化重整行为. 利用所述集成方法获得的最高氢气浓度为99.96vol%和最大转化率为97.1mol%. 此外, 通过含氧化合物的解离、催化重整和水煤气变换反应研究, 探讨了含氧化合物制备纯氢的相关反应路径.

关键词: 含氧化合物, 氢气, 催化重整, 水煤气变换

非对称Ag纳米线三聚体中的等离子体共振及级联效应 489

李跃, 费广涛*, 许少辉, 商国亮, 欧阳浩森, 张立德 (中国科学院合肥物质科学研究院固体物理研究所, 中国科学院材料物理重点实验室, 安徽纳米材料与技术重点实验室, 合肥 230031)

摘要: 本文采用二维有限元方法, 研究了由非对称半径及间距组成的银纳米线三聚体的等离体共振以及异常的电场分布现象. 模拟结果显示, 非对称银纳米线三聚体中存在亮模和暗模. 当亮模分布于两根半径较小的纳米线之间时, 会导致在较大半径的两根纳米线间出现较高的场增强分布, 说明级联效应被抑制. 相反, 当两根半径较小的纳米线之间存在暗模时, 较大的场增强存在于两根较小半径的纳米线间, 此时所产生的级联效应得以实现.

关键词: 非对称三聚体, 暗模和亮模, 消光光谱, 级联效应

1,3-二烷基咪唑离子液体-水二元混合物的溶致显色参数和优先溶剂化行为 497

丁珊, 魏立纲*, 李坤兰, 马英冲 (大连工业大学轻工与化学工程学院, 大连 116034)

摘要: 以1,3-二烷基咪唑离子液体(ILs)-水二元混合物为目标体系, 研究25°C溶质-溶剂和溶剂-溶剂之间相互作用对溶致显色探针分子的优先溶剂化影响. 通过测量4-硝基苯胺、4-硝基苯甲醚和理查德染料的紫外-可见光谱迁移, 得到偶极性/可极性化(π^*)、氢键酸性(α)、氢键碱性(β)和理查德极性参数(E_T^N)等溶致显色经验参数. 研究表明, 离子液体种类和摩尔分数(x_{IL})影响离子液体-水混合物的溶剂性质. 所有研究的体系都表现出非理想特性行为. $x_{IL}=0.1\sim 0.3$, 溶致显色参数偏离理想值最大. 对于大多数二元混合物, π^* 值显示存在协同作用, 而 E_T^N 、 α 和 β 值并没有体现出这一效应. 协同作用程度与染料探针和离子液体种类等研究体系特性有关. 利用优先溶剂化模型深入分析和研究混合物中分子之间相互作用. 优先溶剂化染料探针分子的顺序为: 离子液体>离子液体-水>水.

关键词: 溶致显色参数, 优先溶剂化, 离子液体, 水

基于PPAR α 激动剂的融合药效团模型的构建及评价 508

乔连生, 贺昱魁, 霍晓乾, 蒋彦荻, 陈艳昆, 陈茜, 张燕玲*, 李贞宇 (北京中医药大学中药学院, 中药基础与新药研究重点实验室, 北京 100102)

摘要: 药效团是最常用的虚拟筛选方法之一, 主要包括配体药效团模型和受体药效团模型两大类. 配体药效团通常具有阳性化合物命中率高的优势, 但却具有准确率低的特点, 受体药效团通常具有较强的特异性, 但却具有漏筛率高的问题. 因此, 合理地利用两种类型的药效团的优势, 有效地规避它们的缺点, 是药效团研究与应用的重要方向. 本研究拟基于PPAR α 激动剂探讨融合药效团模型构建的思路与方法. 首先, 分别构建PPAR α 激动剂的配体和受体药效团模型. 通过比较两种药效团模型的药效特征的差异, 确认主要及次要的药效特征. 进一步以受体药效团模型为模板, 调整其主要和次要药效特征的半径及权重, 通过单因素实验及正交试验设计, 获得半径及权重的最优值, 从而构建最优的融合药效团模型. 随后, 融合药效团被用于进一步的中药化学成分PPAR α 激动剂活性预测. 最后, 通过三个化合物数据库的筛选, 评价融合药效团准确性、可靠性和适用性, 并以筛选效率为指标, 比较融合药效团与其他分子模拟模型及筛选方式的优劣. 结果发现, 针对PPAR α 激动剂, 融合药效团模型具有比单一药效团模型更好的筛选效率. 同时, 融合药效团也具有与药效团联合筛选相近的筛选效率, 且具有更好的化合物活性评价能力, 能合理的规避配体药效团与受体药效团计算预测结果不一致的问题. 研究结果显示, 融合药效团模型具有独特的优势, 可以进一步用于化合物生物活性的计算及药物设计研究.

关键词: 融合药效团, 配体药效团, 受体药效团, PPAR α 激动剂, 分子对接, 联合筛选

基于可逆固体氧化物电池堆的电能高效存储 517

甘丽珍^a, 谢奎^{b*} (a. 合肥工业大学机械与汽车工程学院, 合肥 230009; b. 中国科学院福建物质结构研究所, 中国科学院功能纳米结构与组装重点实验室, 福州 350002)

摘要: 研究了固体氧化物电池堆中电能的可逆存储与产生, 通过相变金属存储燃料电池模式下的热能并在电解池模式下加以利用. 系统的荷电状态(即氢燃料百分比)可显著增加开路电压, 系统压力的增加有效提高了开路电压. 较高的系统压力可促进电极表面的物质扩散和输运, 相应地改善电极的极化电阻. 通过有效的热能管理, 系统的电能可逆存储的循环效率可高达92%.

关键词: 可逆固体氧化物电池, 荷电状态, 热能存储, 电能存储, 电能产生